NeuroImage 49 (2010) 2375–2386

Contents lists available at ScienceDirect

NeuroImage

journal homepage: www.elsevier.com/locate/ynimg

Defining functional SMA and pre-SMA subregions in human MFC using resting state fMRI: Functional connectivity-based parcellation method

Jae-Hun Kim [a,b], Jong-Min Lee [a,*], Hang Joon Jo [c], Sook Hui Kim [d], Jung Hee Lee [b], Sung Tae Kim [b], Sang Won Seo [d], Robert W. Cox [c], Duk L. Na [d], Sun I. Kim [a], Ziad S. Saad [c]

[a] Department of Biomedical Engineering, Hanyang University, Seoul 133-791, Republic of Korea
[b] Department of Radiology, Samsung Medical Center, Sungkyunkwan University School of Medicine, Seoul 135-710, Republic of Korea
[c] Scientific and Statistical Computing Core, National Institute of Mental Health, National Institutes of Health, Department of Human and Health Services, 10 Center Drive, Room 1D80, Bethesda, MD 20892-1148, USA
[d] Department of Neurology, Samsung Medical Center, Sungkyunkwan University School of Medicine, Seoul 135-710, Republic of Korea

ARTICLE INFO

Article history:
Received 3 June 2009
Revised 5 October 2009
Accepted 7 October 2009
Available online 23 October 2009

ABSTRACT

Noninvasive parcellation of the human cerebral cortex is an important goal for understanding and examining brain functions. Recently, the patterns of anatomical connections using diffusion tensor imaging (DTI) have been used to parcellate brain regions. Here, we present a noninvasive parcellation approach that uses "functional fingerprints" obtained by correlation measures on resting state functional magnetic resonance imaging (fMRI) data to parcellate brain regions. In other terms, brain regions are parcellated based on the similarity of their connection – as reflected by correlation during resting state – to the whole brain. The proposed method was used to parcellate the medial frontal cortex (MFC) into supplementary motor areas (SMA) and pre-SMA subregions. In agreement with anatomical landmark-based parcellation, we find that functional fingerprint clustering of the MFC results in anterior and posterior clusters. The probabilistic maps from 12 subjects showed that the anterior cluster is mainly located rostral to the vertical commissure anterior (VCA) line, whereas the posterior cluster is mainly located caudal to VCA line, suggesting the homologues of pre-SMA and SMA. The functional connections from the putative pre-SMA cluster were connected to brain regions which are responsible for complex/cognitive motor control, whereas those from the putative SMA cluster were connected to brain regions which are related to the simple motor control. These findings demonstrate the feasibility of the functional connectivity-based parcellation of the human cerebral cortex using resting state fMRI.

Introduction

Noninvasive parcellation of the human cerebral cortex into functionally distinct areas is an important field of neuroscience. Anatomical landmarks such as sulci and gyri are commonly used to delineate cortical areas of interest for the interpretation of functional neuroanatomy (Fischl et al., 2004; Goldstein et al., 1999), with the default assumption that such delineation also reflects functional specialization. However, there is a limited correspondence between sulcal- and gyral-based anatomical boundaries and those based on functional specialization or more fine-grained structural organizations such as cytoarchitecture (Amunts et al., 1999). As an alternative approach, white matter connectional information has been used to delineate distinct brain regions based on the assumption that a unique set of afferent and efferent connections to a given area is crucial factor in determining the functions that the area can perform (Passingham et al., 2002). Recently, diffusion tensor imaging (DTI) has been used for parcellation of the human cerebral cortex on the basis of the anatomical connectivity profiles, called "anatomical fingerprints," in the thalamus (Behrens et al., 2003), medial frontal cortex (Johansen-Berg et al., 2004), and Broca's area (Anwander et al., 2007).

"Functional fingerprints" is another approach that aims to parcellate cortical areas based on the similarity between functional connectivity patterns to other parts of the brain. This has been done with single-cell recordings (Mushiake et al., 1991) in animal studies, and from measurements of receptor architecture (Zilles et al., 2002) in postmortem. Areas that exhibit similar patterns of connectivity are said to have the same functional fingerprint. Invasive electrophysiological recordings in several cortical areas have led to the production of functional fingerprints in animals. However, it is difficult with this approach to record from multiple brain areas at once, and electrophysiological recording cannot be readily used for studying normal

Abbreviations: DTI, diffusion tensor imaging; MFC, medial frontal cortex; SMA, supplementary motor area; VCA, vertical commissure anterior; fMRI, functional magnetic resonance imaging; DMN, default mode network.

* Corresponding author. Sung-dong P.O. Box 55, Seoul 133-605, Korea. Fax: +82 2 2296 5943.
E-mail address: ljm@hanyang.ac.kr (J.-M. Lee).

1053-8119 © 2009 Elsevier Inc. Open access under CC BY-NC-ND license.
doi:10.1016/j.neuroimage.2009.10.016

human brain function. Receptor imaging can provide information on the functional fingerprints of the human brain, with the limitation that this can only be defined postmortem. Here we present a method for noninvasively dividing up a cortical area based on its member voxels' functional fingerprints with connectivity assessed from resting state functional magnetic resonance imaging (fMRI) data.

The majority of fMRI studies infer brain connectivity by modeling fMRI time series in response to the stimuli presented (Heeger and Ress, 2002; Logothetis, 2008). In this approach, the acquisition of data for construction of functional fingerprints has practical limitations, as it is difficult to acquire data on a wide range of areas and over a wide range of tasks. However, resting state fMRI has recently provided an alternative perspective for understanding the function of the brain. Based on brain energy metabolism studies (Raichle, 2006; Raichle and Mintun, 2006), this alternative perspective suggests that the brain has stable patterns of spontaneous activity in the absence of tasks, and these patterns of spontaneous activity provide an alternative approach to understanding brain functional organization (Biswal et al., 1995; Fiser et al., 2004; Kenet et al., 2003; Llinas, 1988; MacLean et al., 2005). Previous resting state studies show that the coherent spontaneous fluctuations are present in a large number of neuroanatomical systems, which include motor, visual, auditory, attention, and language networks (Fox and Raichle, 2007).

Applications of resting state fMRI have recently demonstrated promise in describing boundaries between functional areas in limited regions of cortex in the normal population, and in individual subjects. Margulies et al. (2007) demonstrated more fine-grained functional connectivity patterns of differentiation among anterior cingulate cortex (ACC) subregions than were apparent in task–response fMRI studies (Margulies et al., 2007). Cohen et al. (2008) provided the possibility of functional parcellation of the human brain regions by demonstrating the sharp change of resting state connectivity patterns along the cerebral cortex, even if the distance between cortical seed locations is very close (Cohen et al., 2008). Zhang et al. (2008) demonstrated that the human thalamus can be subdivided into putative nuclei regions based on the strength of functional connectivity from predefined target areas (Zhang et al., 2008).

Inspired by such previous approaches, we developed a functional connectivity-based parcellation method using resting state fMRI. We demonstrate that by using resting state function fingerprints of voxels within an area, we can segment it into different regions.

Materials and methods

Selection of segmentation area

We chose to segment the medial frontal cortex (MFC) using the resting state functional connectivity-based parcellation method detailed below. MFC was chosen because it is thought to be composed of two cytoarchitectonically and functionally distinct regions: the supplementary motor area (SMA) (F3) and the pre-SMA (F6) (Matelli et al., 1985, 1991; Picard and Strick, 1996; Rizzolatti et al., 1996). The SMA holds a complete somatotopical representation of body movement, whereas the pre-SMA holds a cognitive or abstract role in the performance of complex tasks, preparation for movement, motor selection, acquisition of new motor skills, and higher order aspects of speech (Nachev et al., 2008; Picard and Strick, 1996; Tanji, 1996, 2001); therefore, the functional role of the pre-SMA is considered more associated with complex/cognitive control situations than is that of the SMA (Nachev et al., 2008). Furthermore, the structural border between the SMA and pre-SMA is generally defined by the vertical line traversing the anterior commissure (VCA) line (Picard and Strick, 1996, 2001; Rizzolatti et al., 1996; Zilles et al., 1996). This allows us to segment the region based on the structural images from each subject, and provided a reference segmentation with which to compare our results.

Subjects and data acquisition

Twelve right-handed participants (6 males and 6 females; mean age: 22 ± 2 years) were scanned for this study. Echo planar imaging (EPI) was carried out with Philips Intera Achieva 3.0 Tesla scanner equipped with an 8-channel SENSE head coil (Phillips Healthcare, the Netherlands). Whole-brain EPI time series scans (time repetition [TR] = 3000 ms; time echo [TE] = 35 ms; flip angle = 90°; 35 slices; matrix = 128×128; field of view [FOV] = 220×220 mm^2; acquisition voxel size = $1.72 \times 1.72 \times 4$ mm^3) consisted of 155 volumes and lasted for 7.75 min. During each scan, participants were instructed to rest with their eyes open and fixated on a crosshair which was centrally projected in white against a black background. For spatial normalization, localization, and definition of the SMA and pre-SMA, a high-resolution T1-weighted anatomical image was then acquired using a magnetization-prepared gradient echo sequence (TR = 9.9 ms; TE = 4.6 ms; flip angle = 8°; 298 slices; FOV = 240×240 mm^2; acquisition voxel size = $0.5 \times 0.5 \times 0.5$ mm^3). Resting state data were acquired in the axial plane, and anatomical data were aquired in the sagittal plane. These datasets were collected as a part of another study not described here. Informed written consent was obtained from all subjects and the study was approved by the Institutional Review Board of the Samsung Medical Center.

Manual segmentation of the MFC into SMA and pre-SMA

For each subject, the SMA and the pre-SMA were manually defined by one neurologist (S.H. Kim) by tracing gyral and sulcal landmarks that are consistently found across subjects on high-resolution 3D T1-weighted images. The SMA was manually defined as the area of the MFC in the superior frontal gyrus lying dorsal to the cingulate sulcus, rostral to the primary motor cortex, and caudal to the VCA line, whereas the pre-SMA was manually defined as the area of the MFC in the superior frontal gyrus lying dorsal to the cingulate sulcus, rostral to the VCA line, and caudal to the virtual line passing through the genu of the corpus callosum (Picard and Strick, 1996, 2001; Rizzolatti et al., 1996). The seed (MFC) mask for functional parcellation was defined by the union of the two manually defined SMA and pre-SMA masks. These two masks did not overlap and there was no gap between them.

For each subject, a gray matter mask was created by inverse transforming a probabilistic gray matter volume from MNI space to the subject's own space. The probabilistic gray matter mask was FSL's avg152T1_gray mask thresholded at probability 0.3.

Preprocessing of fMRI data

Data preprocessing was carried out using the fMRIB software library (FSL) (www.fmrib.ox.ac.uk). fMRI preprocessing steps consisted of (1) discarding of the first four volumes in each scan series, which were collected before equilibrium magnetization was reached; (2) correction for slice timing; (3) 3D rigid-body correction for head motion within and across runs (this step provided a record of head position within and across all fMRI runs); and (4) intensity scaling of each fMRI run to yield a whole-brain mode value of 1000. No participant had head motion of more than 2.0 mm translation in any of the three directions or more than 2.0° maximum rotation around any of the axes during the resting state scan (Table 1).

Removal of nuisance signals

Functional connectivity analysis was carried out using AFNI (http://afni.nimh.nih.gov/afni/) (Cox, 1996). We preprocessed the fMRI time series for correlation-based functional connectivity analysis (Fox et al., 2005; Vincent et al., 2007) as follows. Data were temporally band-pass filtered ($0.009 \text{ Hz} < f < 0.08 \text{ Hz}$) and spatially smoothed

Table 1
Maximum and average head motion during resting state for each subject.

Subjects	Maximum		Average	
	Displacement (mm)	Rotation (degree)	Displacement (mm)	Rotation (degree)
1	0.47	1.08	0.11	0.17
2	0.90	0.66	0.14	0.17
3	0.36	1.15	0.10	0.21
4	0.41	0.60	0.11	0.18
5	1.10	0.72	0.16	0.14
6	0.94	0.82	0.20	0.12
7	0.38	0.44	0.07	0.08
8	0.67	0.90	0.17	0.13
9	0.60	0.67	0.12	0.15
10	0.55	1.12	0.15	0.18
11	0.40	1.28	0.10	0.20
12	0.41	0.58	0.07	0.11

Average displacement or rotation is calculated as $\frac{\sum_{i=1}^{N} |x(i)| + |y(i)| + |z(i)|}{3N}$, where N is the number of time points, and $x(i), y(i), z(i)$ are head displacement along x, y, z axis or rotation around x, y, z axis.

with a 5 mm full width at half-maximum Gaussian blur. To reduce spurious correlations from cardiac and respiratory fluctuations, subject motion, and other brain spanning common signals (Birn et al., 2006; Macey et al., 2004), we created a set of regressors and regressed them out of the EPI time series. Specifically, the regressors of no interest were (1) global signal averaged over the whole-brain mask, (2) signal averaged over the white matter mask, (3) signal averaged from the ventricular mask, (4) six motion parameters, and (5) their first derivatives.

Functional correlation maps

Functional connectivity between a pair of voxels is represented by the Pearson correlation coefficient between their preprocessed resting state timeseries. To reduce the computational complexity, correlations were computed only between voxels in the gray matter mask. Let $I(x,t)$ be a voxel x's preprocessed resting state timeseries. The cross-correlation coefficient $r_x(v)$ between voxels x and v is given by Eq. (1):

$$r_x(v) = \frac{1/T \sum_{t=1}^{T} \left(I(x,t) - \bar{I}(x)\right)\left(I(v,t) - \bar{I}(v)\right)}{S_I(x) S_I(v)} \quad (1)$$

where $\bar{I}(.)$ and $S_I(.)$ are the mean and standard deviation of $I(.,t)$, respectively. The summation limit, T, corresponds to the total number of time points. Correlation coefficients were then normalized with the application of the Fisher's z transform (Zar, 1996)

$$z_x(v) = 0.5 \times \log \frac{1 + r_x(v)}{1 - r_x(v)} \quad (2)$$

Functional connectivity-based parcellation

The basic idea behind functional connectivity-based parcellation is that voxels from the same functional region have resting signals that correlate in a similar and distinguishable manner with the remaining voxels in the brain. In this first application, we seek to determine the functional subdivision of the MFC area. For each high-resolution ($1.72 \times 1.72 \times 4$ mm^3) EPI voxel x in the MFC area, we calculated a normalized correlation map $z_x(V)$, where V is the whole-brain set of gray matter voxels resampled to a low resolution version ($5 \times 5 \times 5$ mm^3) of the smoothed resting state data. These maps ($z.(V)$) are stored in the rows of **Z**, the 'functional connectivity profile matrix' of dimensions $N_x \times N_v$, where N_x is the number of high-resolution voxels in MFC, and N_v is the number of low-resolution gray matter voxels in the downsampled dataset. The use of the low resolution dataset allowed us to reduce the size of the matrix being analyzed by a factor of 10.5. This downsampling made it easier to perform further computations with matrix **Z**. N_v ranged from 5945 to 8420 voxels. The number of high-resolution voxels (N_x) within MFC was around 1500.

To describe the degree of similarity between functional connectivity maps of voxels in MFC, we computed the 'functional similarity

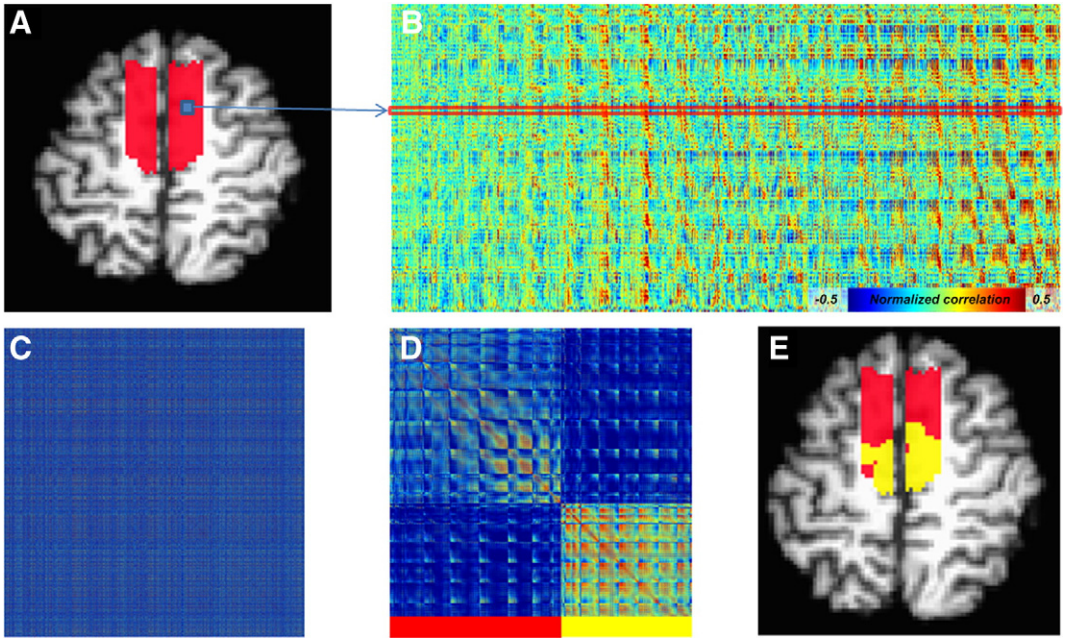

Fig. 1. Functional connectivity-based parcellation of the MFC in a single subject. (A) Manually defined MFC ROI. (B) "Functional connectivity profile (Z) matrix" (number of voxels within MFC × number of voxels within the gray matter). (C) "Functional similarity (S) matrix" (number of voxels within MFC × number of voxels within MFC). (D) "Reordered functional similarity ($\mathbf{S_c}$) matrix" is shown. The clusters defined in $\mathbf{S_c}$ matrices are indicated by the colored bar below the matrices. (E) The image shows the clusters mapped onto the individual brain according to the $\mathbf{S_c}$ matrix. The MFC was parcellated into anterior (red) and posterior (yellow) clusters along the anterior–posterior axis using the same color scheme as the colorbar used in (D).

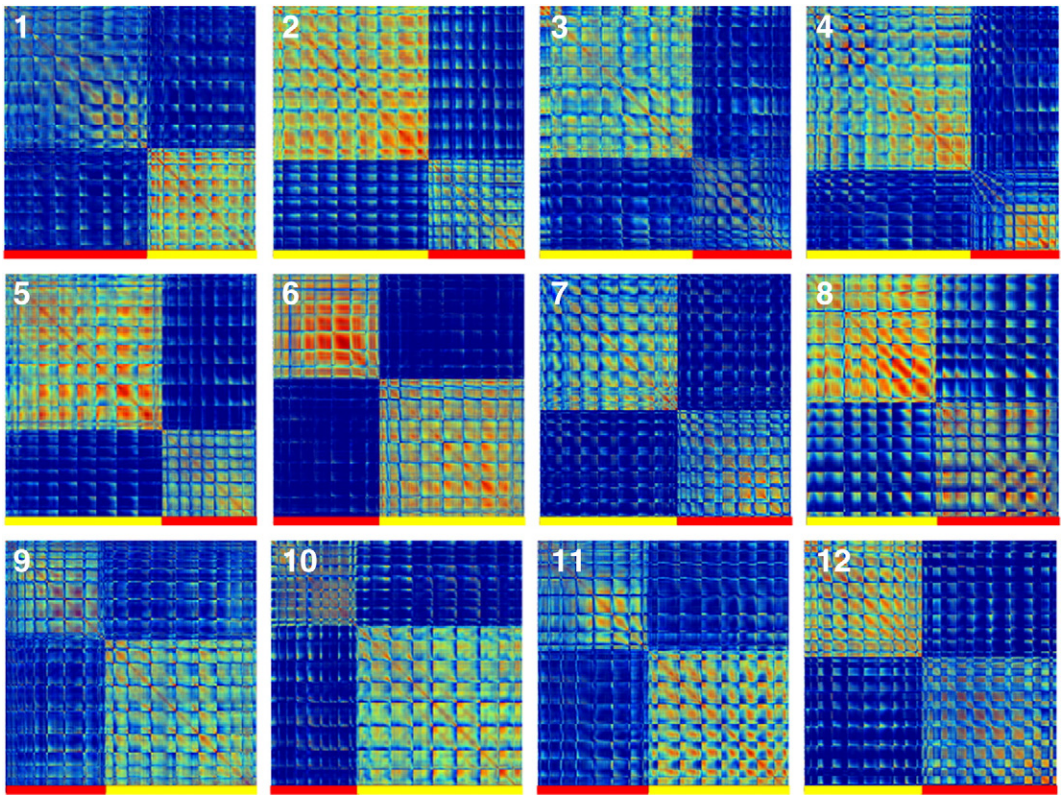

Fig. 2. Reordered functional similarity ($\mathbf{S_c}$) matrices for each of the 12 subjects. The clusters defined in the $\mathbf{S_c}$ matrix are indicated by the colored bar below the matrix.

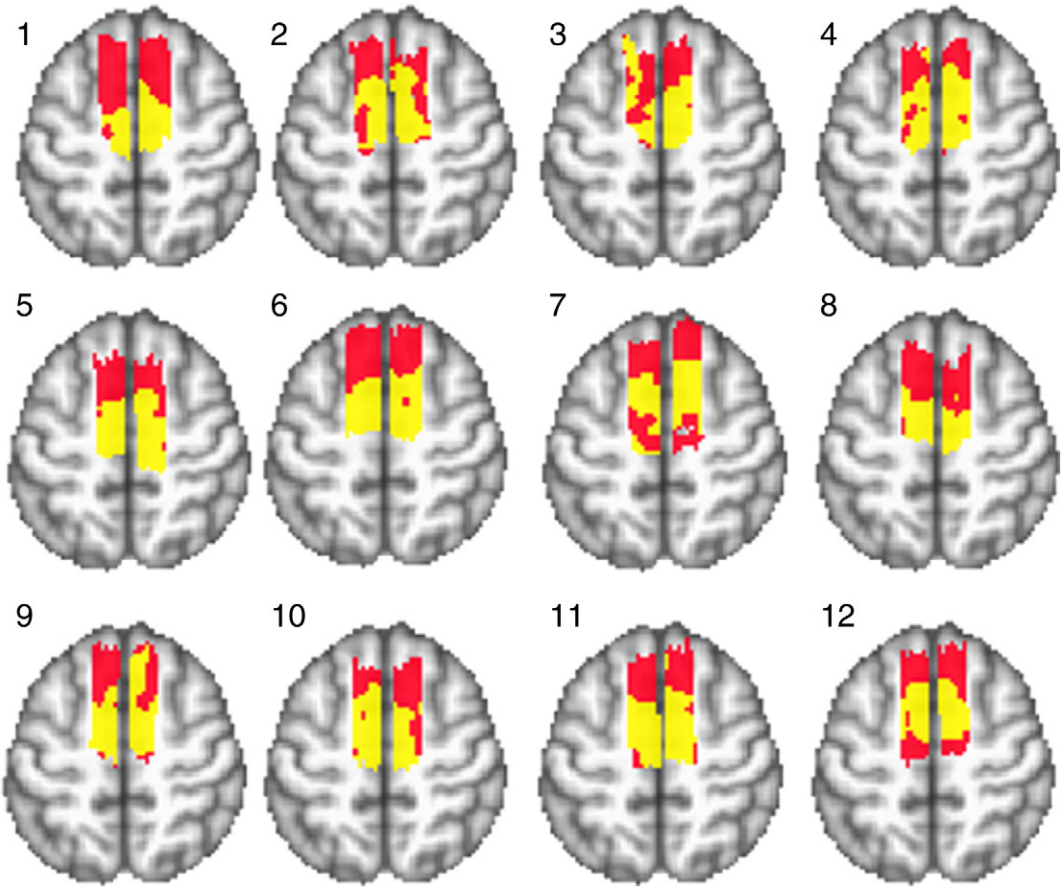

Fig. 3. Reproducibility of functional connectivity-defined clusters between 12 subjects in axial slice ($Z = 58$ in MNI coordinates). The MFC was parcellated into anterior (red) and posterior (yellow) clusters along the anterior–posterior axis. The results in sagittal slice can be found in Supplementary Figs. S1 and S2 ($X = -10$ for left hemisphere and $X = 10$ for right hemisphere in MNI coordinates).

matrix' $\mathbf{S} = 1/N_v(\mathbf{ZZ}')$ which is the cross-correlation matrix of **Z**. Thus, each element (i,j) of this $N_x \times N_x$ matrix characterizes the degree of similarity between the normalized correlation map $z_i(v)$ of MFC voxel i and the normalized correlation map $z_j(v)$ of MFC voxel j. Element (i,j) of **S** measures how similar the whole-brain functional connectivity of MFC voxel i is to that of MFC voxel j. The calculation of **S** also reduces the dimensionality of the data by capturing the similarity of connectedness in a matrix that is a factor of 5 smaller than **Z**, on average. The K-means cluster algorithm ($K = 2$) was then applied to the columns of the **S** matrix, thereby associating each voxel with one of two clusters based on the similarity of their connectedness to the rest of the brain. The reordered functional similarity matrix is termed $\mathbf{S_c}$.

We also tested whether the resultant clustering of **S** was not specific to MFC, but an artifact of some low spatial frequency noise component for which we did not account. This test was done by shifting the manually delineated MFC mask to other arbitrary locations in the brain and recreated $\mathbf{S_c}$ matrices at these new locations.

Functional connectivity maps for each cluster

For each subject, the connectivity map $z_{cluster}(.)$ between one cluster and the brain was created by averaging across the subset of rows of **Z** corresponding to that cluster. These normalized correlation maps describe the whole-brain connectivity pattern common to voxels in each of the clusters. A one sample t-test ($n = 12$ subjects) on these maps was performed to test for areas where the averaged normalized correlation is significantly different from 0 ($p < 0.05$, FDR corrected). These are the areas that are detectably correlated in a similar way to the collection of voxels in a given MFC cluster.

Results

Functional parcellation of the MFC

Fig. 1 summarizes the segmentation process for one subject. A mask of MFC was manually defined on the T1-weighted image (Fig. 1A) and resting state data was used to generate a functional connectivity profile (**Z**) matrix (Fig. 1B) for every voxel in MFC with the rest of the brain. The functional similarity matrix (**S**) was obtained by cross-correlating the **Z** matrix (Fig. 1C) and the reordered functional similarity ($\mathbf{S_c}$) matrix was subsequently created using K-means clustering (Fig. 1D). Each entry in $\mathbf{S_c}$ represents the degree to which a pair of voxels in MFC is similarly connected to the rest of the brain. The tiled pattern in the $\mathbf{S_c}$ matrix reflects the slicewise ordering of voxels in **Z**. Reshuffling this order resulted in the same clustering but without the tiled appearance in the $\mathbf{S_c}$ matrix. Fig. 1E shows a display of cluster membership of each voxel in MFC atop the subject's anatomical image. Note how the clusters are organized into anterior and posterior clusters along the anterior–posterior axis.

Reproducibility between subjects

To explore the reproducibility of the functional connectivity-defined clusters between subjects, we processed data from 12 subjects. Fig. 2 shows that all reordered similarity ($\mathbf{S_c}$) matrices had clearly identifiable breakpoints where the connection similarity profiles changed abruptly. Fig. 3 shows the two clusters to be similarly oriented along the anterior–posterior axis for each of the 12 subjects (Fig. 3 for an axial slice, and Supplementary Figs. S1 and S2 for two sagittal slices). Fig. 4 shows the population probabilistic maps in MNI

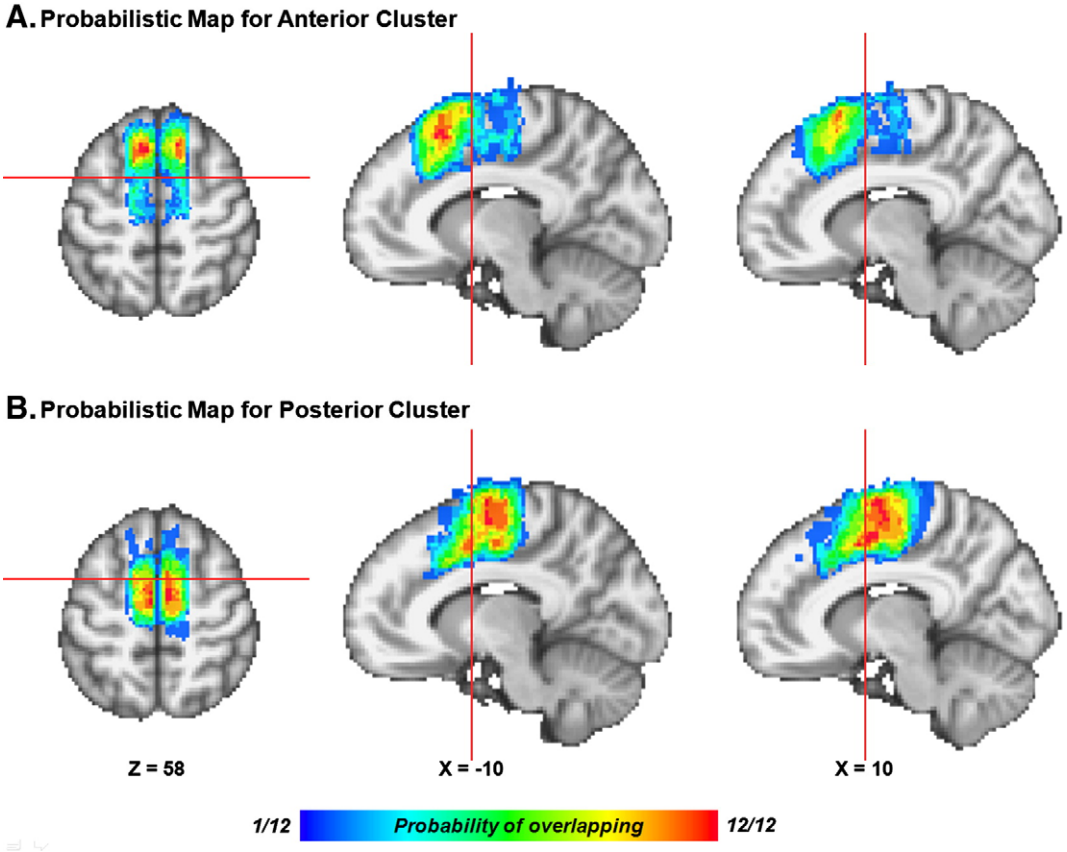

Fig. 4. Probabilistic maps for functional connectivity-defined clusters. (A) Probabilistic map for anterior clusters. (B) Probabilistic map for posterior clusters. The probabilistic maps are presented in the axial ($Z = 58$), left ($X = -10$), and right ($X = 10$) sagittal slices in MNI space. Spatial normalization was done using an affine transformation with nearest neighbor interpolation. The red line indicates $Y = 0$. The color scheme represents the probability of overlapping brains in each voxel across the 12 subjects, from 0 (blue) to 1 (red).

space for each functional connectivity-defined cluster by computing cluster overlap across subjects. The population probabilistic maps showed that most of the anterior clusters were located rostral to the vertical line extending from the anterior commissure ($Y \approx 0$), whereas the most of the posterior clusters were located mainly caudal to the vertical line (Fig. 4). The functional boundary between the anterior and posterior clusters was located close to the VCA line ($Y \approx 0$), which suggests that these functional connectivity similarity clusters correspond to anatomical homologues of pre-SMA and SMA.

Correspondence between structural and functional subregions

There was a good general correspondence between the functional connectivity-based subdivision of MFC and the anatomy-based subdivision of MFC. Fig. 5 shows the correspondence between manual (A) and functional (B) parcellation of MFC for subject number 1. The functionally delineated anterior and posterior clusters corresponded closely to the anatomical landmark-based pre-SMA and SMA, respectively. Fig. 5C is a plot of the centers of mass (CoM) for functional (blue) and anatomical (red) parcellations of anterior and posterior clusters for each of the 12 subjects. Black lines join CoMs from the same subject. The mesh in blue is a dorsal view of the surface model of the hemispheres of one of the subjects, transformed to MNI space. The CoMs for the anatomical pre-SMA colocalized with the CoMs for the functional connectivity-based anterior cluster, whereas the CoMs of the anatomical SMA colocalized with the CoMs of the posterior cluster. Paired two-sample t-tests were performed on distances between functional and anatomical CoMs. For both

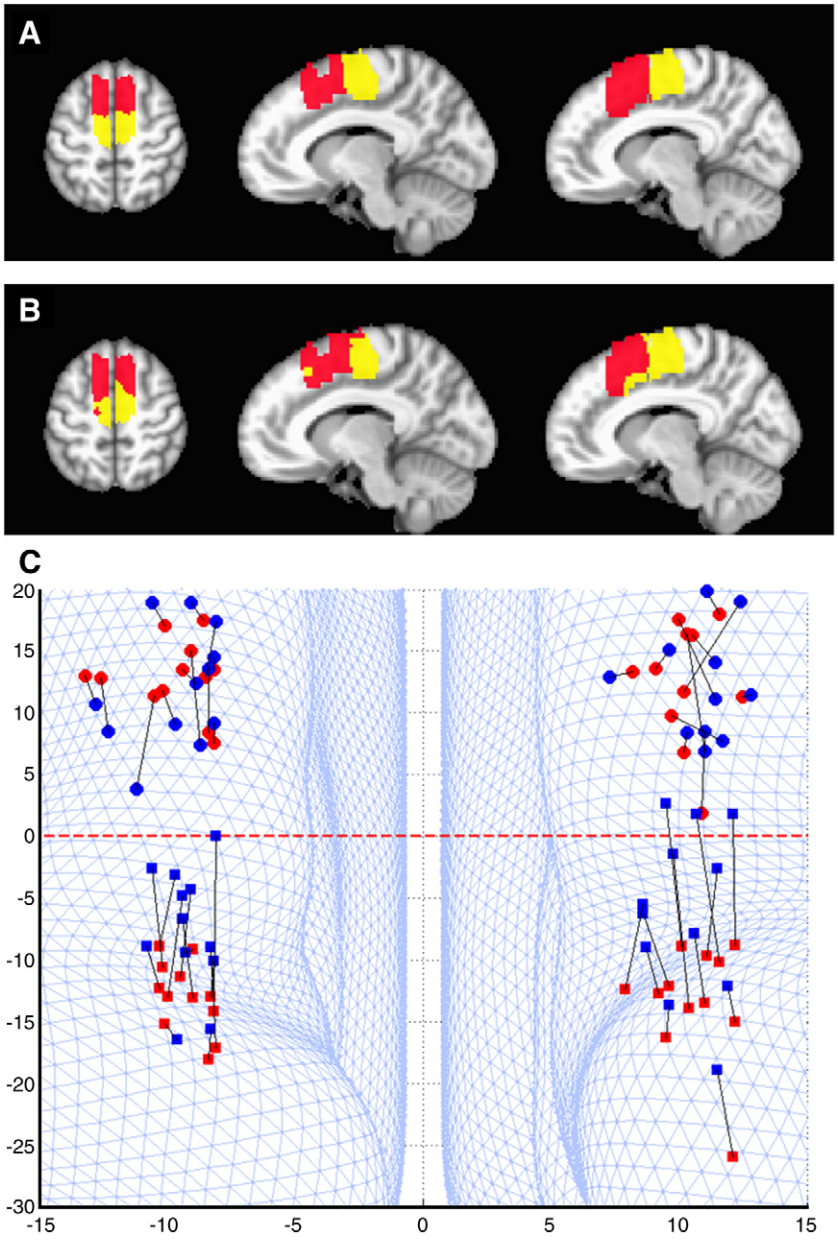

Fig. 5. Test of structure–function correspondences. (A and B) Comparison between anatomically and functionally defined clusters in axial ($Z = 58$), left ($X = -10$), and right ($X = 10$) sagittal slices for subject number 1. For each panel, the images show gyral/sulcal pattern-defined clusters (A) and functional connectivity-defined clusters (B) using the same color scheme used in Fig. 1. (C) Colocalization of anatomically and functionally defined clusters. Each colored point represents the center of mass of the functional connectivity-defined cluster (blue) or anatomic landmark-defined cluster (red) for a single subject. The circle shape represents a center of mass of anterior cluster, and the square shape represents a center of mass of posterior cluster. Black lines connect points from the same individual. The mesh in blue is a dorsal view of the surface model of the hemispheres of one of the subjects, transformed to MNI space. The red dashed line indicates $Y = 0$ in MNI coordinates from the dorsal view.

hemispheres, the average CoM of the anterior cluster was significantly closer to that of the anatomically defined pre-SMA than to that of the anatomically defined SMA, whereas the CoM of the posterior cluster was significantly closer to that of the anatomically defined SMA when compared with that of the anatomically defined pre-SMA ($p<0.001$ in all four tests).

Functional fingerprints for the putative SMA and pre-SMA

Fig. 6 shows the cross-subject averaged normalized correlation maps for the putative pre-SMA (A), and SMA (B). Results are shown with no thresholding because no thresholding was used in creating the connectivity matrices, or in the clustering phase. However, to report on the strongest correlations, we use results from the one sample *t*-test ($p<0.05$, FDR corrrected). The *t*-test showed that for the functional pre-SMA cluster, normalized correlations were significant with regions in the prefrontal cortex, the inferior frontal gyrus, the angular gyrus, and the anterior cingulate cortex. In contrast, for the functional SMA cluster, normalized correlations were significant with regions in the premotor area, the primary motor cortex, the somatosensory cortex, and the middle cingulate cortex. Fig. 7 shows unthresholded similar maps to those in Fig. 6, but for correlation patterns in the subcortical areas. Normalized correlations with functional pre-SMA cluster were higher in the caudate and the anterior thalamus, while for the functional SMA cluster, the normalized correlations were higher in the putamen and the ventrolateral thalamus. Note that these subcortical correlations are lower in magnitude than those seen in the cortical areas of Fig. 6, and most would not reach significance at the levels reported for cortical areas. This may be caused by differences in noise levels, or the relatively high smoothness (5 mm FWHM) and the coarse resolution ($5\times5\times5$ mm) at which the gray matter voxels were resampled.

Clustering results with mask in control regions

We were concerned that the functional parcellation could reflect a spatially smooth noise component for which we did not account, rather than brain connectivity. It is conceivable that spatially smooth noise could result in any ROI being divided into roughly equal parts in the A–P direction with $K=2$ clustering. To address this concern, we repeated the analysis with masks comparable to the one used for MFC but shifted to other brain areas. Such control regions did not produce a clustering pattern similar to the one obtained for MFC. The clusters do not show a division that occurs along the anterior to posterior direction and the clusters are less spatially grouped than they are in

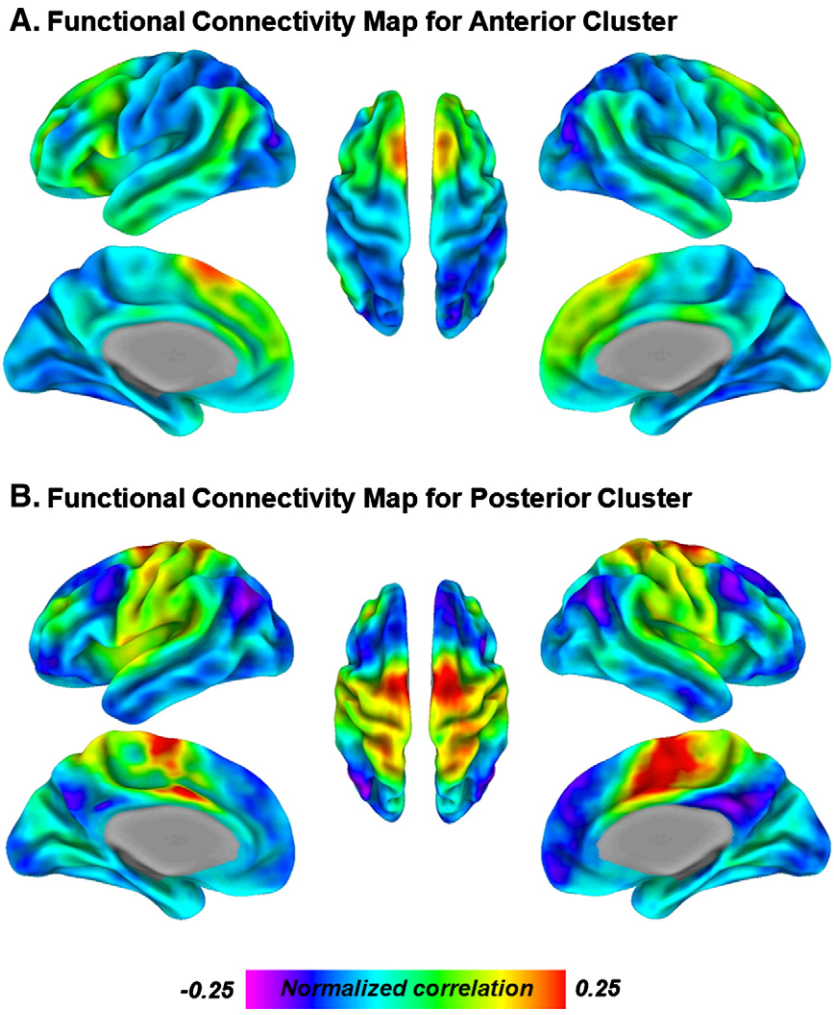

Fig. 6. Cross-subject averaged normalized correlation maps for the anterior and the posterior cluster, projected to a cortical surface model. (A) The anterior cluster is functionally connected to brain regions in the prefrontal cortex, the inferior frontal gyrus, the angular gyrus, and the anterior cingulate cortex. (B) The posterior cluster is functionally connected to brain regions in the premotor area, the primary motor cortex, the somatosensory cortex, and the middle cingulate cortex. The colorscale shows the average normalized correlation with the cluster $z_{cluster}(.)$, with *z* values ranging from negative (−0.25) to positive (0.25). Data are displayed on the lateral and medial surfaces of the left hemisphere (left), the dorsal surface (center), and the lateral and medial surfaces of the right hemisphere (right).

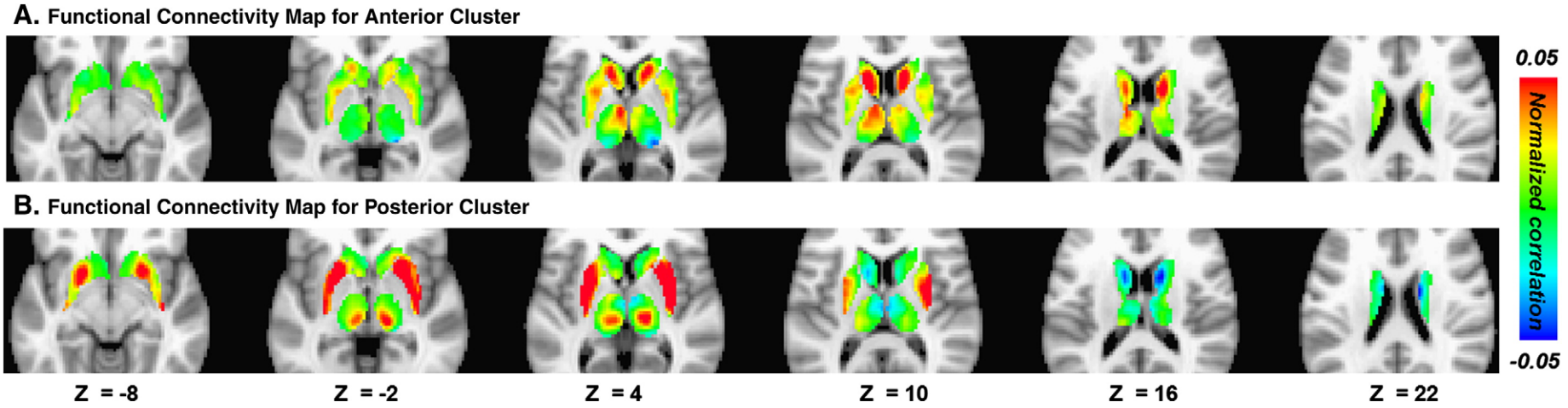

Fig. 7. Cross-subject averaged normalized correlation maps for the anterior and the posterior cluster, masked to show only the subcortex. (A) The anterior cluster is more strongly correlated with subcortical regions in the caudate and the anterior thalamus. (B) The posterior cluster is more strongly correlated with subcortical regions in the putamen and the ventrolateral thalamus. The colorscale shows the average normalized correlation with the cluster $z_{cluster}(.)$, with z values ranging from negative (−0.05) to positive (0.05). The range in the colorscale is different from the one in Fig. 6 to highlight differences in the spatial patterns of correlation. Z coordinate is in MNI space.

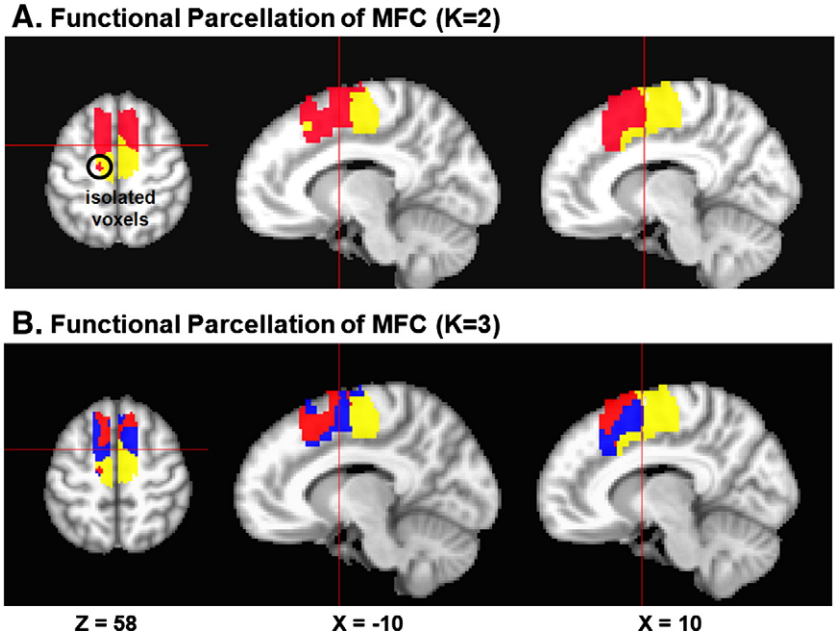

Fig. 8. The results of functional parcellation of MFC depending on external parameter (K = the number of cluster). (A) Functional parcellation of MFC at $K=2$. The black circle highlights isolated voxels. (B) Functional parcellation of MFC at $K=3$. The red line marks the plane $Y=0$.

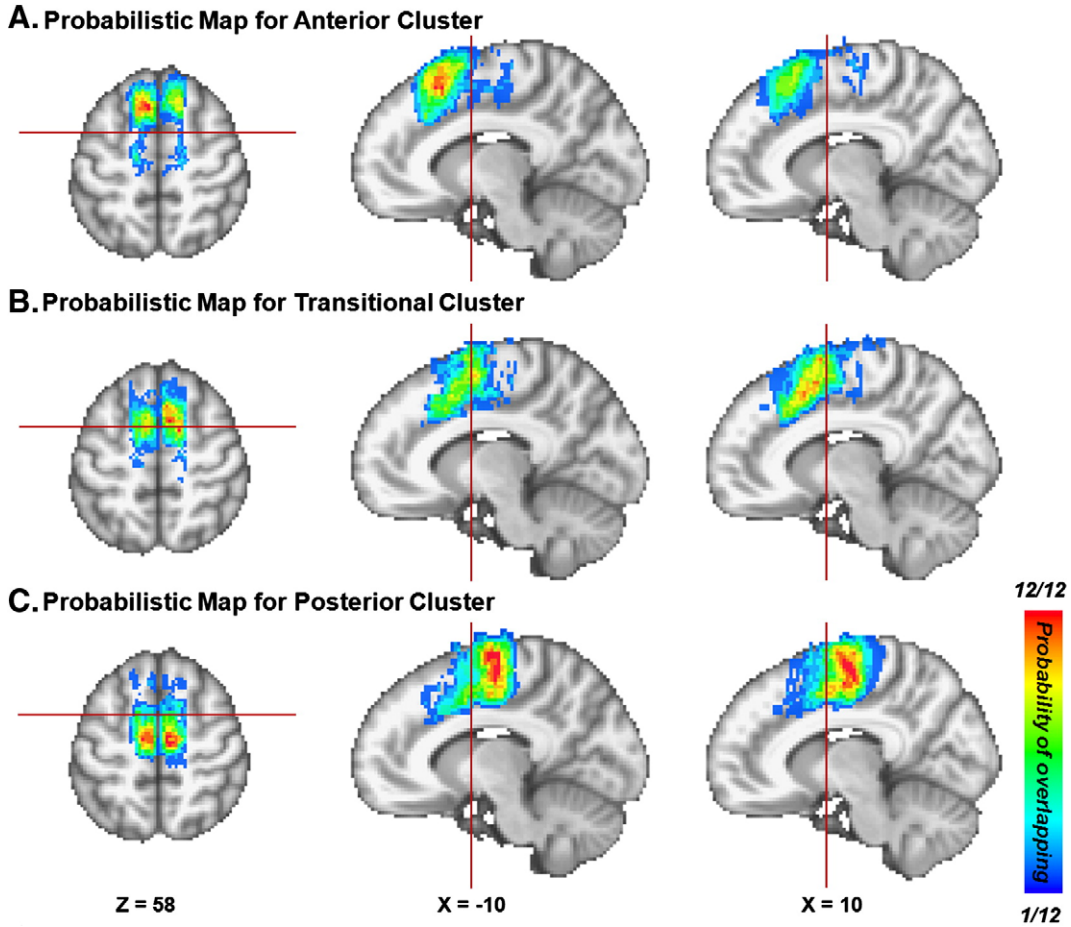

Fig. 9. Probabilistic maps for functional connectivity-defined clusters ($K=3$). (A) Probabilistic map for anterior clusters. (B) Probabilistic map for transitional clusters. (C) Probabilistic map for posterior clusters. The probabilistic maps are presented in the axial ($Z=58$), left ($X=-10$), and right ($X=10$) sagittal slices in MNI space. Spatial normalization was done using affine transformation with nearest neighbor interpolation method. The red line indicates $Y=0$. The color scheme represents the probability of overlapping brains in each voxel across the 12 subjects, from 0 (blue) to 1 (red).

MFC. Supplementary Fig. S3 contains $\mathbf{S_c}$ matrices and functional connectivity-defined clusters for various control regions.

Discussion

We have segmented a brain region into areas with different whole-brain functional fingerprints from resting state fMRI. The functional fingerprints were used to parcellate the human MFC into anterior and posterior clusters. In agreement with manual gyral-based segmentation, the probabilistic map of anterior clusters from 12 subjects was located rostral to the VCA line, and that of posterior clusters was located caudal to the VCA line, suggesting the anatomical homology of pre-SMA and SMA. These findings show that the functional connectivity patterns from resting state fMRI can be a reliable feature for noninvasive parcellation of the human cerebral cortex. In addition, the proposed method could be useful for examining intrinsically organized neuroanatomical systems of brain subregions as illustrated in Figs. 6 and 7.

Isolated voxels in MFC and functional parcellation of MFC ($K=3$)

The reordered functional similarity ($\mathbf{S_c}$) matrices show identifiable breakpoints where functional connectivity patterns changed abruptly. Most of voxels belonging to the same cluster in $\mathbf{S_c}$ matrix formed one contiguous spatial cluster in the brain. However, this was not always the case. As illustrated in Fig. 8A, we found isolated voxels in the middle of the spatial cluster. These isolated voxels may have been incorrectly classified because of noise, or because our method forcibly classified all MFC voxels into one of the two cluster ($K=2$). If by using a higher K the spatially isolated subcluster blends into its neighbors, this would suggest that the area is perhaps better subdivided into more regions. However, when applying K-means clustering with $K=3$, we found that these voxels did not form a spatially contiguous third cluster, suggesting that their presence may be due to noise or artifacts. It is not obvious how the number of clusters should be chosen a priori for a particular area of interest. For MFC, the choice of two clusters was based on previous practice. However, using three clusters reveals a more subtle subdivision that may be as valid as with $K=2$. More recently, cytoarchitectonic evidence suggested that the MFC could be divided into three subregions (Vorobiev et al., 1998). Analyzing all 12 subjects with $K=3$ showed that the MFC was parcellated into anterior, transitional, and posterior clusters along the anterior–posterior axis (Fig. 9). The functional connectivity-based parcellation of MFC for $K=3$ seems to be consistent across subjects, but further study is needed to quantify the structure–function correspondence with such cytoarchitectonic maps. It would be informative to conduct experiments in the same set of subjects comparing tractography-based parcellations (Johansen-Berg et al., 2004) and resting state based as shown here. The two approaches could be complimentary, with more specificity provided by DTI where tracts are easily discerned and our resting state approach where fiber crossing is a problem.

Control seed ROIs

In this project, we chose the MFC complex, which has reliable anatomical markers (Brodmann's area 6). Despite the match with manual segmentation of MFC, we were concerned that the subdivision of MFC into two clusters of comparable size reflected some spatially smooth property of the data. With a smooth random field, placing a mask in any region and requiring two clusters may end up splitting the area into two spatially contiguous parts of comparable size. However, when the mask was moved around the brain we found that the two clusters were no longer as spatially contiguous or organized along a particular direction. This finding, along with the distinct connectivity patterns shown in Figs. 6 and 7, suggests that the clustering result reflects true connectivity differences found in MFC.

We tried to apply our method using the whole brain as a seed mask, but we could not parcellate the whole brain into subregions because of computational power and memory problem. With larger computational power and improvements to the algorithm, and perhaps with longer resting state data acquisitions, our approach should be applicable to a whole-brain mask, which would allow the investigation and parcellation of whole-brain resting state functional networks.

Functional connections of SMA and pre-SMA in the resting brain

The current results confirm observations from previous functional and anatomical connectivity studies and provide comprehensive knowledge related to pre-SMA and SMA networks. It is known that the functional role of the pre-SMA is associated with more complex and cognitive controls, such as alternation of motor plans, task switching, acquisition of new motor skills, and motor selection, when compared with the SMA (Marsden et al., 1996; Nachev et al., 2008; Picard and Strick, 1996). Studies using task-related functional data demonstrated that the pre-SMA is coactivated with prefrontal cortex and caudate when comparing task switching with task-repetition (Gu et al., 2008), and that the pre-SMA is coactivated with ACC during a Stroop task (Barch et al., 2001; Pardo et al., 1990). Anatomical studies using diffusion data demonstrated that the pre-SMA has many projections to and from the prefrontal areas and caudate, whereas the SMA is mainly connected to the primary motor cortex and putamen (Johansen-Berg et al., 2004; Lehericy et al., 2004a,b). These subcortical anatomical connections are reflected by the patterns of Fisher-normalized correlations between anterior and posterior cluster to subcortical regions. The anterior cluster had a high degree of connection to the dorsal caudate, whereas the posterior cluster had a high degree of connection to the putamen. This is generally consistent with evidence that the putamen is the main motor function unit and the dorsal caudate is the main cognitive function unit in the human striatum (Di Martino et al., 2008; Postuma and Dagher, 2006). In our data, connections with subcortical areas were weaker than those with cortical areas. Although these weak correlation patterns play a role in the clustering approach, voxelwise correlations do not reach significance at the level reported for cortical areas. This is likely caused by higher noise levels, size of the structures relative to the smoothness of 5 mm FWHM imposed on the data, and the small number of subjects ($n=12$) for such a statistical test. For this reason, it is not possible to compare our connectivity patterns' subtle spatial details with those from high-resolution anatomy-based data, such as from Lehericy et al. (2004a). For such comparisons to be made, we would need to smooth more carefully within subcortical structures masks (e.g., with AFNI's 3dBlurInMask, or 3danisosmooth) that are created on a per subject basis (Fischl et al., 2002). We would also need more subjects to gain statistical power. Nonetheless, the overall connectivity patterns in our current results do agree with previous findings and reveal the comprehensive networks of pre-SMA and SMA observed over a wide range of tasks and from diffusion data.

Resting state functional conditions

In this study, the connectivity patterns distinguishing pre-SMA from SMA were obtained from resting state data that were acquired during eyes open with fixation. However, resting state data are often acquired during eyes closed conditions, or with eyes open and no fixation target. Studies have shown that the functional connectivity differences exist between different resting state conditions (Bianciardi et al., 2009; Zou et al., 2009). For example, Yan et al. (2009) found that the functional connectivity of the default mode network (DMN) in the resting state with the eyes open is significantly higher than that with the eyes closed, but the functional connectivity patterns were similar across the different resting state conditions.

Other studies showed that functional connectivity patterns of the DMN were similar across the different resting state conditions (Fox et al., 2005; Greicius et al., 2003).

Based on these studies, it seems that differences due to the eyes being open or closed are ones of connectivity strength, rather than spatial pattern. Since we found that pre-SMA and SMA had different connectivity patterns, we expect that the results would hold during conditions of eyes closed, or eyes open without fixation. However, it is possible that resting condition design may have an effect when this type of connectivity mapping in cortical areas more closely involved in visual processing (e.g., frontal eye fields).

Possible impact of global signal regression

The use of global signal regression has recently been under debate. Fox et al. (2009) demonstrated that global signal regression leads to improvement in the correspondence between resting state functional correlation and anatomy (e.g., cortical–thalamic correlations). Murphy et al. (2009), on the other hand, demonstrated that global signal regression leads to not only over-estimation of negative correlation, but also under-estimation of positive correlation. We have included global signal regression in our study because it has been common practice until these recent controversies. The bias this introduces is not expected to differentially affect connectivity from SMA, compared to that from pre-SMA, so we expect that global signal regression should not affect our results. To test this, we repeated the analysis without the global signal regressor. Average signals from each of white matter and CSF were left as regressors of no interest to account for non-gray matter specific correlations. We found the probabilistic maps of Fig. 4 obtained with global signal regression were very similar to these maps obtained without global signal regression (Fig. S4).

Conclusion

We have proposed a method for segmenting a specific region into subregions based on its voxels' whole-brain functional fingerprints. The subdivisions are determined without explicit reference to anatomical landmarks and require no cognitive tasks during fMRI acquisition. The ability to localize functional SMA and pre-SMA *in vivo* could be used not only to examine abnormal functional networks related to motor function, but also to more precisely target functional motor areas in the treatment of movement disorders, such as patients with SMA epilepsy and alien-limb syndrome, by functional neurosurgery.

Acknowledgments

We thank the two reviewers of our manuscript for their detailed and constructive feedback. This work was supported by the Korea Science and Engineering Foundation (KOSEF) NRL program grant funded by the Korea government (MEST) (R0A-2007-000-20068-0). R.W. Cox and Z.S. Saad are supported by the Division of Intramural Research, National Institute of Mental Health, and National Institute of Neurological Disorders and Stroke.

Appendix A. Supplementary data

Supplementary data associated with this article can be found, in the online version, at doi:10.1016/j.neuroimage.2009.10.016.

References

Amunts, K., Schleicher, A., Burgel, U., Mohlberg, H., Uylings, H.B., Zilles, K., 1999. Broca's region revisited: cytoarchitecture and intersubject variability. J. Comp. Neurol. 412, 319–341.
Anwander, A., Tittgemeyer, M., von Cramon, D.Y., Friederici, A.D., Knosche, T.R., 2007. Connectivity-based parcellation of Broca's area. Cereb. Cortex 17, 816–825.
Barch, D.M., Braver, T.S., Akbudak, E., Conturo, T., Ollinger, J., Snyder, A., 2001. Anterior cingulate cortex and response conflict: effects of response modality and processing domain. Cereb. Cortex 11, 837–848.
Behrens, T.E., Johansen-Berg, H., Woolrich, M.W., Smith, S.M., Wheeler-Kingshott, C.A., Boulby, P.A., Barker, G.J., Sillery, E.L., Sheehan, K., Ciccarelli, O., Thompson, A.J., Brady, J.M., Matthews, P.M., 2003. Non-invasive mapping of connections between human thalamus and cortex using diffusion imaging. Nat. Neurosci. 6, 750–757.
Bianciardi, M., Fukunaga, M., van Gelderen, P., Horovitz, S.G., de Zwart, J.A., Duyn, J.H., 2009. Modulation of spontaneous fMRI activity in human visual cortex by behavioral state. NeuroImage 45, 160–168.
Birn, R.M., Diamond, J.B., Smith, M.A., Bandettini, P.A., 2006. Separating respiratory-variation-related fluctuations from neuronal-activity-related fluctuations in fMRI. NeuroImage 31, 1536–1548.
Biswal, B., Yetkin, F.Z., Haughton, V.M., Hyde, J.S., 1995. Functional connectivity in the motor cortex of resting human brain using echo-planar MRI. Magn. Reson. Med. 34, 537–541.
Cohen, A.L., Fair, D.A., Dosenbach, N.U., Miezin, F.M., Dierker, D., Van Essen, D.C., Schlaggar, B.L., Petersen, S.E., 2008. Defining functional areas in individual human brains using resting functional connectivity MRI. NeuroImage 41, 45–57.
Cox, R.W., 1996. AFNI: software for analysis and visualization of functional magnetic resonance neuroimages. Comput. Biomed. Res. 29, 162–173.
Di Martino, A., Scheres, A., Margulies, D.S., Kelly, A.M., Uddin, L.Q., Shehzad, Z., Biswal, B., Walters, J.R., Castellanos, F.X., Milham, M.P., 2008. Functional connectivity of human striatum: a resting state fMRI study. Cereb. Cortex 18, 2735–2747.
Fischl, B., Salat, D.H., Busa, E., Albert, M., Dieterich, M., Haselgrove, C., van der Kouwe, A., Killiany, R., Kennedy, D., Klaveness, S., Montillo, A., Makris, N., Rosen, B., Dale, A.M., 2002. Whole brain segmentation: automated labeling of neuroanatomical structures in the human brain. Neuron 33, 341–355.
Fischl, B., van der Kouwe, A., Destrieux, C., Halgren, E., Segonne, F., Salat, D.H., Busa, E., Seidman, L.J., Goldstein, J., Kennedy, D., Caviness, V., Makris, N., Rosen, B., Dale, A.M., 2004. Automatically parcellating the human cerebral cortex. Cereb. Cortex 14, 11–22.
Fiser, J., Chiu, C., Weliky, M., 2004. Small modulation of ongoing cortical dynamics by sensory input during natural vision. Nature 431, 573–578.
Fox, M.D., Raichle, M.E., 2007. Spontaneous fluctuations in brain activity observed with functional magnetic resonance imaging. Nat. Rev., Neurosci. 8, 700–711.
Fox, M.D., Snyder, A.Z., Vincent, J.L., Corbetta, M., Van Essen, D.C., Raichle, M.E., 2005. The human brain is intrinsically organized into dynamic, anticorrelated functional networks. Proc. Natl. Acad. Sci. U. S. A. 102, 9673–9678.
Fox, M.D., Zhang, D., Snyder, A.Z., Raichle, M.E., 2009. The global signal and observed anticorrelated resting state brain networks. J. Neurophysiol. 101, 3270–3283.
Goldstein, J.M., Goodman, J.M., Seidman, L.J., Kennedy, D.N., Makris, N., Lee, H., Tourville, J., Caviness Jr., V.S., Faraone, S.V., Tsuang, M.T., 1999. Cortical abnormalities in schizophrenia identified by structural magnetic resonance imaging. Arch. Gen. Psychiatry 56, 537–547.
Greicius, M.D., Krasnow, B., Reiss, A.L., Menon, V., 2003. Functional connectivity in the resting brain: a network analysis of the default mode hypothesis. Proc. Natl. Acad. Sci. U. S. A. 100, 253–258.
Gu, B.M., Park, J.Y., Kang, D.H., Lee, S.J., Yoo, S.Y., Jo, H.J., Choi, C.H., Lee, J.M., Kwon, J.S., 2008. Neural correlates of cognitive inflexibility during task-switching in obsessive-compulsive disorder. Brain 131, 155–164.
Heeger, D.J., Ress, D., 2002. What does fMRI tell us about neuronal activity? Nat. Rev., Neurosci. 3, 142–151.
Johansen-Berg, H., Behrens, T.E., Robson, M.D., Drobnjak, I., Rushworth, M.F., Brady, J.M., Smith, S.M., Higham, D.J., Matthews, P.M., 2004. Changes in connectivity profiles define functionally distinct regions in human medial frontal cortex. Proc. Natl. Acad. Sci. U. S. A. 101, 13335–13340.
Kenet, T., Bibitchkov, D., Tsodyks, M., Grinvald, A., Arieli, A., 2003. Spontaneously emerging cortical representations of visual attributes. Nature 425, 954–956.
Lehericy, S., Ducros, M., Krainik, A., Francois, C., Van de Moortele, P.F., Ugurbil, K., Kim, D.S., 2004a. 3-D diffusion tensor axonal tracking shows distinct SMA and pre-SMA projections to the human striatum. Cereb. Cortex 14, 1302–1309.
Lehericy, S., Ducros, M., Van de Moortele, P.F., Francois, C., Thivard, L., Poupon, C., Swindale, N., Ugurbil, K., Kim, D.S., 2004b. Diffusion tensor fiber tracking shows distinct corticostriatal circuits in humans. Ann. Neurol. 55, 522–529.
Llinas, R.R., 1988. The intrinsic electrophysiological properties of mammalian neurons: insights into central nervous system function. Science 242, 1654–1664.
Logothetis, N.K., 2008. What we can do and what we cannot do with fMRI. Nature 453, 869–878.
Macey, P.M., Macey, K.E., Kumar, R., Harper, R.M., 2004. A method for removal of global effects from fMRI time series. NeuroImage 22, 360–366.
MacLean, J.N., Watson, B.O., Aaron, G.B., Yuste, R., 2005. Internal dynamics determine the cortical response to thalamic stimulation. Neuron 48, 811–823.
Margulies, D.S., Kelly, A.M., Uddin, L.Q., Biswal, B.B., Castellanos, F.X., Milham, M.P., 2007. Mapping the functional connectivity of anterior cingulate cortex. NeuroImage 37, 579–588.
Marsden, C.D., Deecke, L., Freund, H.J., Hallett, M., Passingham, R.E., Shibasaki, H., Tanji, J., Wiesendanger, M., 1996. The functions of the supplementary motor area. Summary of a workshop. Adv. Neurol. 70, 477–487.
Matelli, M., Luppino, G., Rizzolatti, G., 1985. Patterns of cytochrome oxidase activity in the frontal agranular cortex of the macaque monkey. Behav. Brain Res. 18, 125–136.
Matelli, M., Luppino, G., Rizzolatti, G., 1991. Architecture of superior and mesial area 6 and the adjacent cingulate cortex in the macaque monkey. J. Comp. Neurol. 311, 445–462.
Murphy, K., Birn, R.M., Handwerker, D.A., Jones, T.B., Bandettini, P.A., 2009. The impact of global signal regression on resting state correlations: are anti-correlated networks introduced? NeuroImage 44, 893–905.

Mushiake, H., Inase, M., Tanji, J., 1991. Neuronal activity in the primate premotor, supplementary, and precentral motor cortex during visually guided and internally determined sequential movements. J. Neurophysiol. 66, 705–718.
Nachev, P., Kennard, C., Husain, M., 2008. Functional role of the supplementary and pre-supplementary motor areas. Nat. Rev., Neurosci. 9, 856–869.
Pardo, J.V., Pardo, P.J., Janer, K.W., Raichle, M.E., 1990. The anterior cingulate cortex mediates processing selection in the Stroop attentional conflict paradigm. Proc. Natl. Acad. Sci. U. S. A. 87, 256–259.
Passingham, R.E., Stephan, K.E., Kotter, R., 2002. The anatomical basis of functional localization in the cortex. Nat. Rev., Neurosci. 3, 606–616.
Picard, N., Strick, P.L., 1996. Motor areas of the medial wall: a review of their location and functional activation. Cereb. Cortex 6, 342–353.
Picard, N., Strick, P.L., 2001. Imaging the premotor areas. Curr. Opin. Neurobiol. 11, 663–672.
Postuma, R.B., Dagher, A., 2006. Basal ganglia functional connectivity based on a meta-analysis of 126 positron emission tomography and functional magnetic resonance imaging publications. Cereb. Cortex 16, 1508–1521.
Raichle, M.E., 2006. Neuroscience: the brain's dark energy. Science 314, 1249–1250.
Raichle, M.E., Mintun, M.A., 2006. Brain work and brain imaging. Annu. Rev. Neurosci. 29, 449–476.
Rizzolatti, G., Luppino, G., Matelli, M., 1996. The classic supplementary motor area is formed by two independent areas. Adv. Neurol. 70, 45–56.
Tanji, J., 1996. New concepts of the supplementary motor area. Curr. Opin. Neurobiol. 6, 782–787.
Tanji, J., 2001. Sequential organization of multiple movements: involvement of cortical motor areas. Annu. Rev. Neurosci. 24, 631–651.
Vincent, J.L., Patel, G.H., Fox, M.D., Snyder, A.Z., Baker, J.T., Van Essen, D.C., Zempel, J.M., Snyder, L.H., Corbetta, M., Raichle, M.E., 2007. Intrinsic functional architecture in the anaesthetized monkey brain. Nature 447, 83–86.
Vorobiev, V., Govoni, P., Rizzolatti, G., Matelli, M., Luppino, G., 1998. Parcellation of human mesial area 6: cytoarchitectonic evidence for three separate areas. Eur. J. Neurosci. 10, 2199–2203.
Yan, C., Liu, D., He, Y., Zou, Q., Zhu, C., Zuo, X., Long, X., Zang, Y., 2009. Spontaneous brain activity in the default mode network is sensitive to different resting-state conditions with limited cognitive load. PLoS ONE 4, e5743.
Zar, J.H. (Ed.), 1996. Biostatistical analysis. Prentice-Hall, Upper Saddle River, New Jersey.
Zhang, D., Snyder, A.Z., Fox, M.D., Sansbury, M.W., Shimony, J.S., Raichle, M.E., 2008. Intrinsic functional relations between human cerebral cortex and thalamus. J. Neurophysiol. 100, 1740–1748.
Zilles, K., Schlaug, G., Geyer, S., Luppino, G., Matelli, M., Qu, M., Schleicher, A., Schormann, T., 1996. Anatomy and transmitter receptors of the supplementary motor areas in the human and nonhuman primate brain. Adv. Neurol. 70, 29–43.
Zilles, K., Palomero-Gallagher, N., Grefkes, C., Scheperjans, F., Boy, C., Amunts, K., Schleicher, A., 2002. Architectonics of the human cerebral cortex and transmitter receptor fingerprints: reconciling functional neuroanatomy and neurochemistry. Eur. Neuropsychopharmacol. 12, 587–599.
Zou, Q., Long, X., Zuo, X., Yan, C., Zhu, C., Yang, Y., Liu, D., He, Y., Zang, Y., 2009. Functional connectivity between the thalamus and visual cortex under eyes closed and eyes open conditions: a resting-state fMRI study. Hum Brain Mapp. 30, 3066–3078.